PAPER

Light triggered interfacial damage self-healing of poly(p-phenylene benzobisoxazole) fiber composites

To cite this article: Zhen Hu *et al* 2018 *Nanotechnology* **29** 185602

IOP Publishing Nanotechnology

Nanotechnology **29** (2018) 185602 (11pp) https://doi.org/10.1088/1361-6528/aab010

Light triggered interfacial damage self-healing of poly(p-phenylene benzobisoxazole) fiber composites

Zhen Hu[1,5], Qing Shao[1], Yudong Huang[1], Long Yu[1], Dayu Zhang[1], Xirong Xu[1], Jing Lin[2,5], Hu Liu[3,4] and Zhanhu Guo[4,5]

[1] School of Chemistry and Chemical Engineering, MIIT Key Laboratory of Critical Materials Technology for New Energy Conversion and Storage, Harbin Institute of Technology, Harbin 150001, People's Republic of China
[2] School of Chemistry and Chemical Engineering, Guangzhou University, Guangzhou 510006, People's Republic of China
[3] National Engineering Research Center for Advanced Polymer Processing Technology, Zhengzhou University, Zhengzhou 450002, People's Republic of China
[4] Integrated Composites Laboratory (ICL), Department of Chemical and Biomolecular Engineering, University of Tennessee, Knoxville, TN 37996, United States of America

E-mail: huzhen@hit.edu.cn, linjing@gzhu.edu.cn and zguo10@utk.edu

Received 11 December 2017, revised 31 January 2018
Accepted for publication 16 February 2018
Published 9 March 2018

Abstract

The interfacial microcracks in the resin matrix composites are difficult to be detected and repaired. However, the self-healing concept provides opportunities to fabricate composites with unusual properties. In the present study, photothermal conversion Ag–Cu_2S nanoparticles were immobilized onto poly(p-phenylene benzobisoxazole) (PBO) fibers via a polydopamine chemistry. Benefitting from the photothermal effects of Ag–Cu_2S, the obtained PBO fibers (Ag–Cu_2S–PBO) efficiently converted the light energy into heat under Xenon lamp irradiation. Then, single PBO fiber composites were prepared using thermoplastic polyurethane as the matrix. It was found that the interfacial damage caused by single fiber pull-out was simply self-healed by Xe light irradiation. This wonderful interfacial damage self-healing property was mainly attributed to the *in situ* heating generation via photothermal effects of Ag–Cu_2S in the composite interface. This paper reports a novel strategy to construct advanced composites with light-triggered self-healing properties, which will provide inspiration for preparing high performance composite materials.

Supplementary material for this article is available online

Keywords: light triggered self-healing, interfacial damage, PBO fibers, photothermal effects, surface modification

(Some figures may appear in colour only in the online journal)

1. Introduction

Polymer composites tend to experience a premature failure due to the formation of cracks or microcracks during the repeated thermomechanical loading [1]. In polymer composite materials, the 'interphase', namely the interfacial region between reinforcing material (fiber or filler) and matrix, is regarded as a critical element in controlling the overall performance of the composites [2–5]. Its major function is to maintain stress transfer from the weak polymer matrix to the strong reinforcing material and to assure durability of composite material. Actually, stress concentration

[5] Authors to whom any correspondence should be addressed.

and micro-crack formation often occur and then propagate in this region, leading to a failure of the composite materials [5, 6]. These cracks are usually unpredictable so that they are difficult to be detected or costly to be repaired [7]. Consequently, how to avoid or repair the interfacial microcracks becomes a hot topic in the area of composite materials [5]. Inspired by the biological systems [8–10], the self-healing concept is applied to composite science to increase the service life of the materials [2, 6, 11]. Although some significant progress has been made in the self-healing systems including gels, polymeric and supramolecular materials over the past decade [8, 12, 13], self-healing presents significant technical challenges in the field of fiber-reinforced composite materials because of stringent manufacturing and performance requirements. It is still a great challenge to develop a facile strategy to fabricate multi-functional interface with self-healing properties [14].

Until now, several approaches have been developed to prepare self-healing materials or structures [12], such as capsule-based methods [15, 16] and microvascular networks [17]. Besides a few specific systems, most materials need external energy stimulus to launch the self-healing process. Owing to the feature of light energy, such as easily achievable, inexpensive [18], unparalleled remote activation and spatial control [19], the light-triggered self-healing materials have received widespread attention [20, 21]. In recent decades, the study of nano/microparticle-mediated photothermal effects has emerged as a particularly attractive topic due to the unique light-to-heat conversion properties [22–27]. The photothermal materials can strongly absorb light, and convert it to heatthat causes a raise in the temperature of the crack zone; then the new covalent or non-covalent bonds will be formed to trigger self-healing in the microcrack area. In fact, the photothermal effects induced self-healing has been achieved by using the rearrangement of thermosensitive bonding, such as Diels–Alder reactions [28] and ligand-metal binding [29]. More interesting, the elevated temperature caused by photothermal effects reduces the viscosity and further allows an effective diffusion of the polymers in the crack. It means that the photothermal effect-based strategy could be an option for self-healing of high T_g polymers. However, common methods often require the polymers to possess a low T_g and sufficient chain mobility at room temperature. To fabricate light triggered self-healing interface, the immobilization of appropriate photothermal agents on the fibers is a key problem that needs to be solved.

Poly(p-phenylene benzobisoxazole) (PBO) fibers are characterized by high thermal stability, high stiffness, and high tensile strength (TS), which are the representation of high-performance fibers and have a great potential to be applied as reinforcement in the composites [30, 31]. Noteworthy, a feasible and high efficient strategy for interfacial treatment could obviously improve the interfacial properties [32]. Owing to their large specific surface area and unique electronic, magnetic and other related properties, nanoparticles are commonly used for surface modification in the field of fiber reinforced polymer composites [33, 34]. Besides that, some semiconductor nanoparticles have been proven to be promising candidates as new generation of photothermal agent. For example, copper sulfide (chalcocite, Cu_2S) [35–37] has attracted increasing attention because of its strong photothermal effect, good photostability, low toxicity, synthetic simplicity and low cost [38, 39]. However, it is difficult to decorate the PBO fibers with nanoparticles due to the chemical inertness of the PBO surface [40]. Until now, several surface modification methods, such as sizing coating [41], seed-mediated adsorption, chemical vapor deposition [42], hydrothermal process [43], electrochemical deposition [44], gamma-ray irradiation, plasma modification, acid treatment, and coupling agent [45], have been employed to improve the interface properties of the PBO composites. However, it is still a great challenge to develop a facile and nondestructive route to modify the surface properties of PBO fibers.

The present study reveals a novel and facile approach to fabricate light-triggered self-healing interface, which also enhances the overall performance of the composites without negatively affecting the initial properties. As the plasmonic coupling between metal nanostructures and semiconductors can enhance the near-field at the metal nanoparticle surface [22, 46], the Ag and Cu_2S nanoparticles are selected and anchored onto the PBO fibers to exert synergistic photothermal properties [47–49]. To immobilize the Ag nanoparticles onto PBO fibers, dopamine is used as the adhesive and reducing agent for reducing silver ions into metallic silver by microwave-assisted chemical reduction technique [50–52]. Then, Ag–PBO fiber is coated with Cu_2S through hydrothermal process. The Ag–Cu_2S nanoparticles on the interface of the composites convert the light energy to heat, which significantly elevates the interfacial temperature, reduces viscosity, and allows effective diffusion of the resins in the crack region [18–20]. Self-healing can be finally achieved by re-fusing the thermoplastic matrix resin to self-heal the interface damage. In the present study, the synthetic procedure of Ag–Cu_2S–PBO fibers is illustrated in figure 1.

2. Experimental methods

2.1. Materials

The PBO fibers with a single filament diameter of 11 μm were purchased from Toyobo Ltd, Japan. Dopamine, tris(hydroxymethyl)aminomethane, acetone, silver nitrate ($AgNO_3$), copper(II) chloride dehydrate ($CuCl_2 \cdot 2H_2O$, 99%), ammonia solution ($NH_3 \cdot H_2O$, 26%) and thiourea (99%) were supplied by Aladdin Reagent Company (Shanghai, PR China). Thermoplastic polyurethane (TPU, $T_g \geqslant 95\,^{\circ}C$, $T_f \geqslant 120\,^{\circ}C$) was obtained from the Shanghai Tongthda hot melt adhesive chemical company. Before use, the PBO fibers were extracted with acetone at 65 °C for 48 h. Other chemicals were used as received without any treatment.

2.2. Preparation of PDA coated PBO fibers

The PDA–PBO fibers were synthesized following the reaction method described previously [40]. Briefly, dopamine

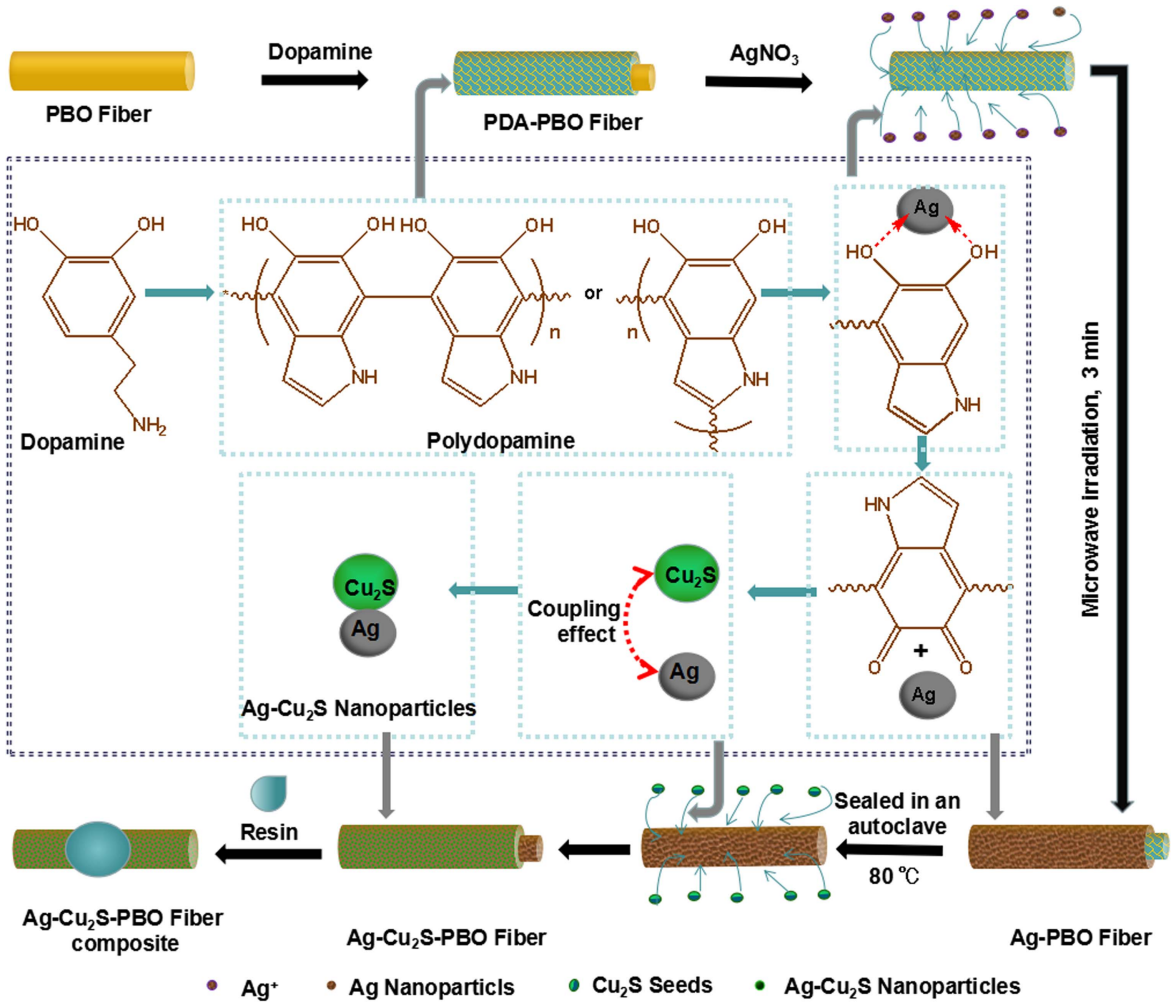

Figure 1. The synthetic route for the preparation of Ag–Cu_2S–PBO fibers.

(0.1–0.3 g) was added into 100 ml tris(hydroxymethyl)aminomethane buffer solution (pH: 8.5–9.0). The PBO fibers were then soaked in the dopamine solution at room temperature for 23 h. The modified PBO fibers (PDA–PBO) were then washed with water to remove unreacted dopamine.

2.3. Immobilization of Ag and Cu_2S nanoparticles on PBO fibers

In order to immobilize the Ag nanoparticles onto PBO fibers, the dopamine was used as adhesive and reducing agent for reducing silver ions to metallic silver. The PDA–PBO fibers were immersed in the solution of $AgNO_3$ (2.5 g l^{-1}, 200 ml). The mixture solution was exposed to high intense microwave irradiation (800 W) for 3 min. After washing with water and drying in air, the Ag coated PBO fibers were obtained (Ag–PBO).

Hydrothermal process was used to deposit the Cu_2S onto the Ag–PBO fibers. Briefly, the Cu_2S seeds were synthesized according to the previously reported procedures [52]. A thiourea solution (20 ml, 1 mol l^{-1}) was dripped into the mixed solution of $CuCl_2$ (20 ml, 0.4 mol l^{-1}) and $NH_3 \cdot H_2O$ (40 ml, 25%–28%) with continuous stirring. The Ag–PBO fibers were then immersed in the above Cu_2S seeds solution. The mixture was sealed in an autoclave heated at 80 °C for 2 h. The obtained fibers (Ag–Cu_2S–PBO) were washed with the dilute HCl and dried in air.

2.4. Characterization of the modified PBO fibers

A Rigaku D/Max-2500 x-ray diffractometer (XRD) using a Cu target radiation source was employed to record XRD data. Ultraviolet–visible spectra (UV–vis) were collected on a SHIMADZU 3100 UV–vis spectrophotometer. X-ray photoelectron spectroscopy (XPS) spectra were recorded using a PHI 5700 ESCA System spectrometer. The scanning electron microscopy (SEM) with a primary electron energy of 3 kV was used to measure the surface morphologies of the fibers. Atomic force microscope (AFM) measurements were performed on a Bruker Dimension Icon.

Single fiber tensile testing was carried out by an electronic mechanical universal material testing machine (Instron 5500R, USA) according to the ASTM D3379-75. More than 60 specimens were examined for each sample, and then the data were analyzed with Weibull statistical method. Interfacial strength testing instrument (Tohei Sanyon Co., Ltd, Japan) was employed to examine the interfacial shear strength (IFSS) between the PBO fibers and epoxy matrix. The

crosshead displacement rate of was 0.06 mm min^{-1}. For each specimen, the data were the average of five to seven specimens (the detailed description is shown in the supporting information, which is available online at stacks.iop.org/NANO/29/185602/mmedia). The test of single fiber pull-out was performed by pulling out a fiber from the cured resin droplet. The IFSS was then determined by the following equation:

$$\mathrm{IFSS} = \frac{F_{\max}}{\pi dl},$$

where $F_{\max}$ represents the maximum load, l represents the embedded length of single filament in epoxy resin, and d represents the average diameter of PBO fibers.

2.5. The evaluation of the photothermal effects of Ag–Cu_2S nanoparticles

In order to measure the photothermal conversion efficiency, the Xenon lamp (500 W) was used as the energy source positioned vertically downward to the surface of the Ag–Cu_2S (100 ml, 1.25 g l^{-1}) solution (the detailed synthetic process of Ag–Cu_2S nanoparticles is shown in the supplementary information). 100 ml pure water was set as the control sample. The temperature was maintained at room temperature and measured with the thermocouple every 10 min.

2.6. The light triggered interfacial self-healing of Ag–Cu_2S–PBO fiber composites

To examine the interfacial self-healing properties of Ag–Cu_2S–PBO fiber composites, the single fiber composites were prepared. Polyurethanes have unique properties in terms of their physical and chemical properties. Compared to other common matrices, the low glass transition temperature and melting point of thermoplastic polyurethane (TPU) make the whole system much easier to achieve photo-thermal self-healing. Furthermore, TPU has good adhesive properties so that it can form a strong bond with the surface of the fibers. The melting transparent TPU was dropped onto the single Ag–Cu_2S–PBO fiber to form a light permeable microdroplet wrapped in the fiber. In order to ensure that the fiber was fully wetted by TPU, the single fiber composites were heated to 180 °C for another 10 min. Then, the debond damage of the composites was achieved by single fiber pull-out test. To trigger the photothermal self-healing, a Xenon lamp (500 W) was positioned 30 cm from the samples and irradiated for a certain time. The IFSS of the self-healed Ag–Cu_2S–PBO fiber composites was recorded by single fiber pull-out test. The self-healing efficiency (ν) was calculated by equation:

$$\nu = \frac{\mathrm{IFSS}}{\mathrm{IFSS}_{\mathrm{origin}}}.$$

3. Results and discussion

The morphologies of the modified PBO fibers were firstly characterized using SEM and optical photograph. As shown in figure 2(a), the surface of pristine PBO fibers was neat and smooth. It is known that the PBO fibers are difficult to be directly coated by the metal ions without modification. Dopamine is believed to be able to adhere onto the surfaces of almost all materials. Moreover, dopamine can also serve as a green reducing agent. Therefore, to immobilize Ag or Cu_2S nanoparticles on the surface of PBO fibers, PDA was firstly coated on the PBO surface. After PDA modification (figure 2(b)), the obtained PBO fibers were covered with a rough polymer film. As observed in figure 2(c), PBO fibers were densely and firmly covered by several circular-like Ag nanoparticles with homogenized sizes after the microwave radiation. Moreover, the immobilization of Ag nanoparticles also changed the color of fibers from deep yellow to light black (figures S1(a)–(c)). It was reported that the plasmon-to-exciton/plasmon coupling effect between the Ag and Cu_2S nanoparticles would enhance the absorption over a broadband wavelength range [51–53]. In order to promote the photothermal conversion, Cu_2S nanoparticles were further introduced to the Ag–PBO fibers, which changed the color of fibers from light black to green (figures S1(c), (d)). As shown in figure 2(d), the Ag–Cu_2S–PBO fibers showed a considerably rough surface which was attributed to the deposition of Ag–Cu_2S nanoparticles. Compared with Ag–PBO fibers, the size of nanoparticles increased and the shape of nanoparticles changed, which further suggested a successful coating of the Cu_2S on the Ag–PBO fibers surface. In order to demonstrate the role of PDA in the immobilization of Ag or Cu_2S nanoparticles, a small part of the PBO fiber surface was carefully controlled not to be modified with PDA. The results revealed that the unmodified surface of PBO fibers was not coated with Ag or Cu_2S nanoparticles after the microwave radiation and following hydrothermal process (figure 2(e)). This result further demonstrated that PDA was an effective adhesive and reducing agent during the growth of the Ag or Cu_2S nanoparticles. Further insight was gained regarding the distributions of the Ag–Cu_2S nanoparticles, and the results were shown in figures 2(f)–(i). The results showed that the Cu, S and Ag elements were evenly distributed on the fibers surface. All of the above results demonstrated Ag–Cu_2S nanoparticles have been successfully coated on the PBO fibers.

The surface morphology and roughness were further observed by AFM (figure 3). As shown in figure 3(a), the surface of pristine PBO fibers was rather smooth without visible irregularity. However, it can be found that plenty of attachments were distributed on the surface of PDA–PBO, Ag–PBO, and Ag–Cu_2S–PBO fibers (figures 3(b)–(d)). The arithmetic mean roughness (Ra) of pristine PBO fibers was 137 nm, which was increased to 149 nm for the PDA–PBO fibers due to the existence of PDA nanofilm. After depositing Ag nanoparticles, a layer of uniform spherical Ag nanoparticles was generated on the fiber surface and led to the increased of Ra to 159 nm. Compared to Ag–PBO fibers, the size of nanoparticles on the Ag–Cu_2S–PBO surface increased significantly, leading to a sharp increase in Ra from 159 to 325 nm. Furthermore, the shape of the nanoparticles has been changed slightly. These results indicated that the Ag–Cu_2S

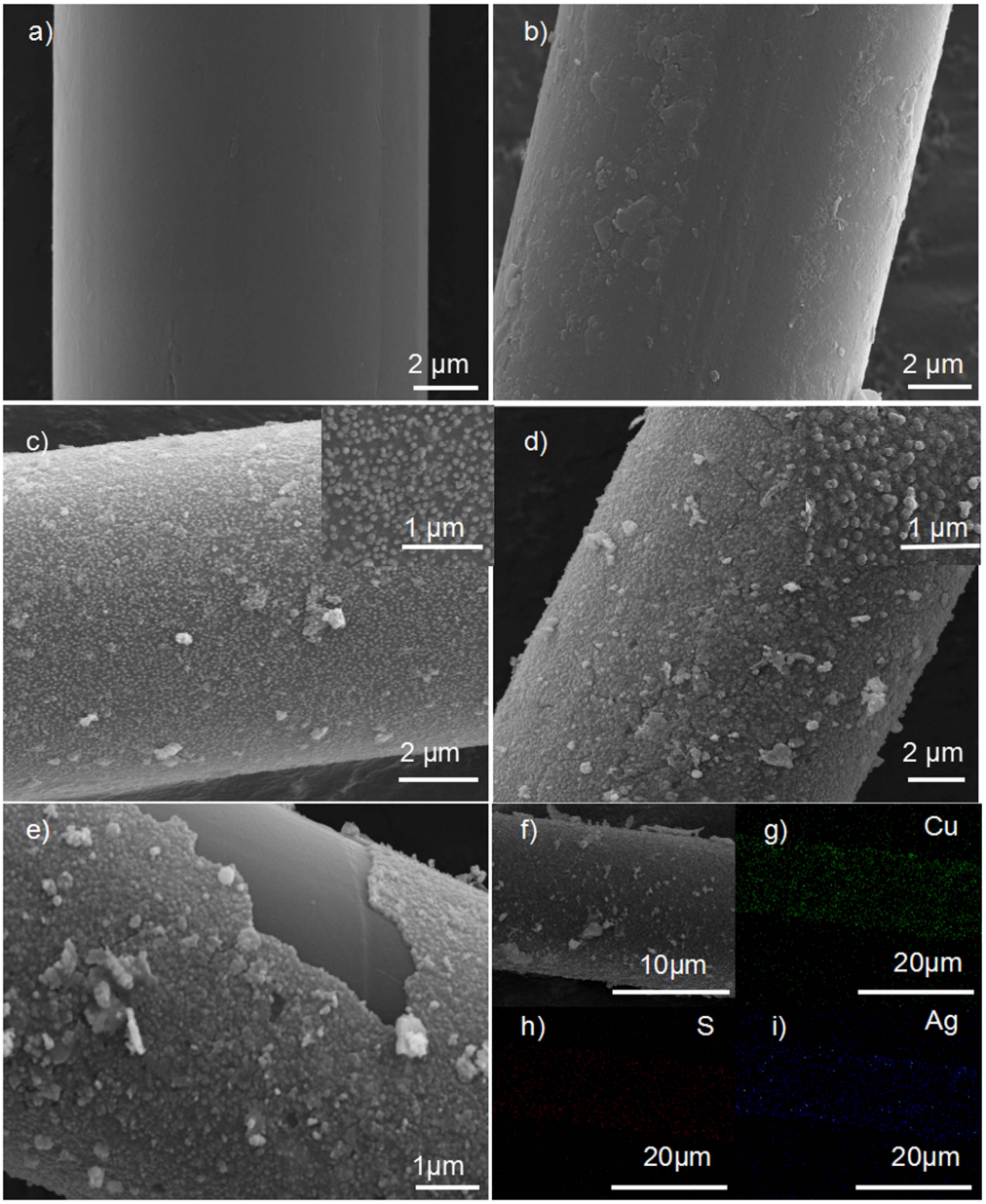

Figure 2. SEM images of the modified PBO fibers: (a) PBO, (b) PDA–PBO, (c) Ag–PBO, and (d) Ag–Cu_2S–PBO; (e) SEM images of the controlled Ag–Cu_2S–PBO fibers; EDX elemental mappings of Ag–Cu_2S–PBO fibers: (f) original SEM image, (g) Cu element, (h) S element, and (i) Ag element.

nanoparticles might play major roles in the improvement of self-healing and interface properties of the PBO fibers [54].

XPS was recorded to examine the chemical composition of the PBO fiber surface. It can be found that both the untreated and treated PBO fibers were comprised of carbon, oxygen and nitrogen elements (figures 4, S2–S5). As shown in table S1 and figures S2–3, the percentage of C and N elements in PDA–PBO fibers was increased which was attributed to the formation of PDA nanofilm. After coated with Ag nanoparticles, new peaks appeared at 371.1 and 377.2 eV corresponding to the Ag 3d (figure S4). Compared with the Ag–PBO fibers, several additional peaks were emerged at 932.5, 952.6 and 162.9 eV in the XPS spectrum of Ag–Cu_2S–PBO fibers, illustrating the presence of metallic Cu and S, respectively (figure S5). Furthermore, the XPS analysis revealed that the atomic ratio of the elements Cu and S in Ag–Cu_2S–PBO fibers was 1:1.65 which was close to the stoichiometry of Cu_2S (table S1). The result demonstrated that Cu_2S nanoparticles were successfully coated on the Ag–PBO fibers. To certify the coupling effect between Ag and Cu_2S nanoparticles, the Ag 3d XPS spectra were observed (figure 4(b)). Compared with the Ag–PBO fibers, the obvious red-shift for the Ag 3d peak was detected for the Ag–Cu_2S–PBO fibers. The plasmonic coupling between Ag and Cu_2S nanoparticles may cause electron transfer from Ag to Cu_2S nanoparticles. The electron transfer further leads the increase of carrier concentration in Ag and the enhancement of the absorption band.

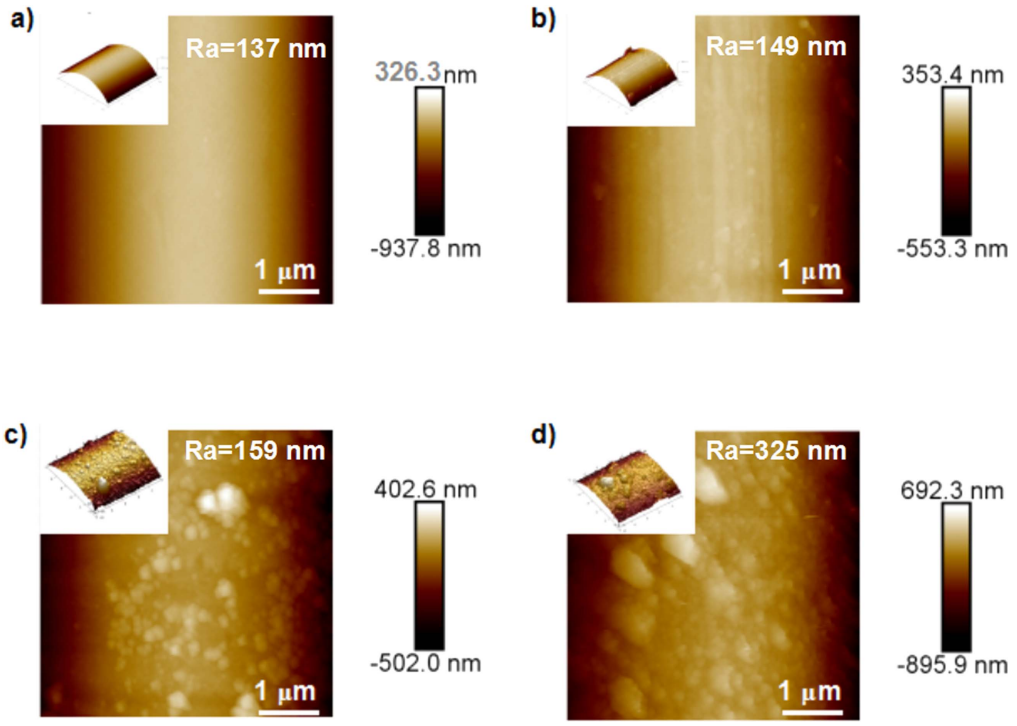

Figure 3. AFM images of the modified PBO fibers: (a) PBO, (b) PDA–PBO, (c) Ag–PBO, and (d) Ag–Cu_2S–PBO. The insets are the 3D images of the fibers. Ra indicates the surface roughness of the fibers.

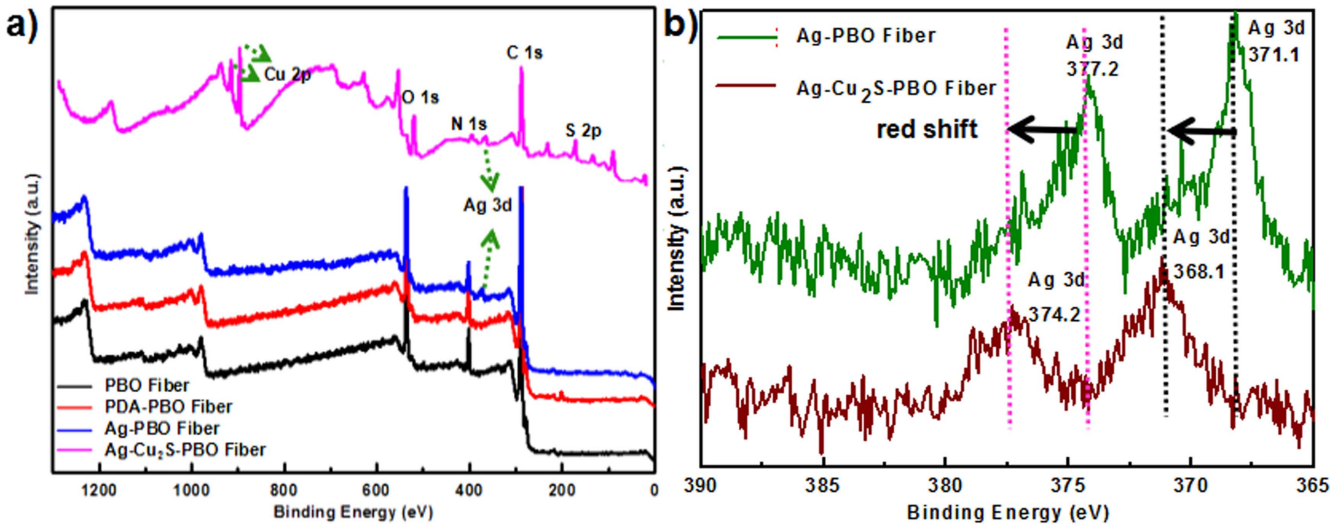

Figure 4. The XPS spectra of (a) PBO, PDA–PBO, Ag–PBO and Ag–Cu_2S–PBO fibers; (b) high-resolution Ag 3d XPS spectra of Ag–PBO and Ag–Cu_2S–PBO fibers.

In the XRD pattern of PBO fibers (figure 5), there were two typical diffraction peaks at 16.1° and 26.5° corresponding to 'side-by-side' (200) and 'face-to-face' (010) distance between two PBO chains, respectively [55]. The XRD pattern of PDA–PBO fibers was similar to PBO, indicating that the rigid crystal structure of PBO was largely maintained. Compared with pristine PBO fibers, the XRD pattern of the Ag–PBO fibers revealed the distinct peaks at 38.1°, 40.8°, 44.3°, 51.3°, 64.3°, 67.5°, 76.7°, 78.02°, 80.9°, 83.6° and 87.2°, consistent with the (004), (101), (1, −1, 2), (103), (104), (110), (112), (201), (202), (203) and (108) planes of the hexagonal phase Ag with *cell parameters* $a = b = 2.8862$ Å, $c = 10.0$ Å (JCPDS no. 411402) (figures 5, S6(a)). Furthermore, the diffraction peaks of Ag–Cu_2S–PBO fibers appeared at 7.4°, 10.1°, 37.3°, 42.0°, 45.3° and 48.4°, consistent with the (011), (111), (034), (413), (−544) and (106) planes of the monoclinic phase Cu_2S with cell parameters $a = 15.235$ Å, $b = 11.885$ Å, $c = 13.496$ Å (JCPDS no. 330490) (figures 5, S6(b)). To better observe the microstructures of the Ag–Cu_2S–PBO fibers, the high-resolution TEM (HRTEM) images of the single Ag–Cu_2S–PBO fibers composites were observed and shown in the inset of figure 5. In the HRTEM images, the crystalline lattice of both Ag and Cu_2S

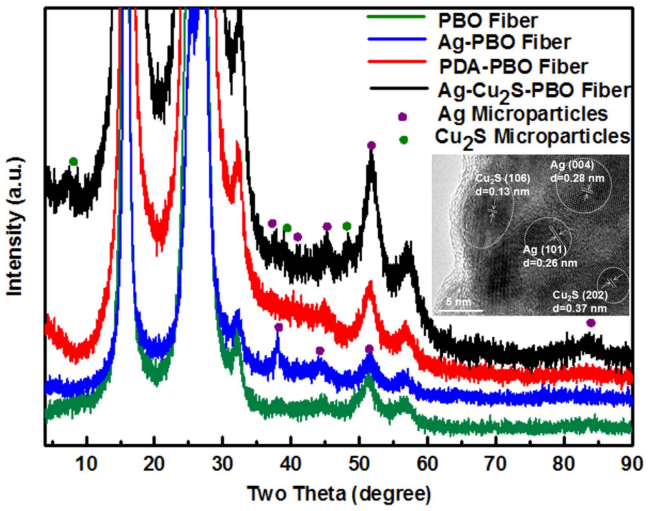

Figure 5. XRD patterns of PBO, Ag–PBO, PDA–PBO, and Ag–Cu_2S–PBO fibers. The inset is the representative HRTEM image of the Ag–Cu_2S–PBO fibers.

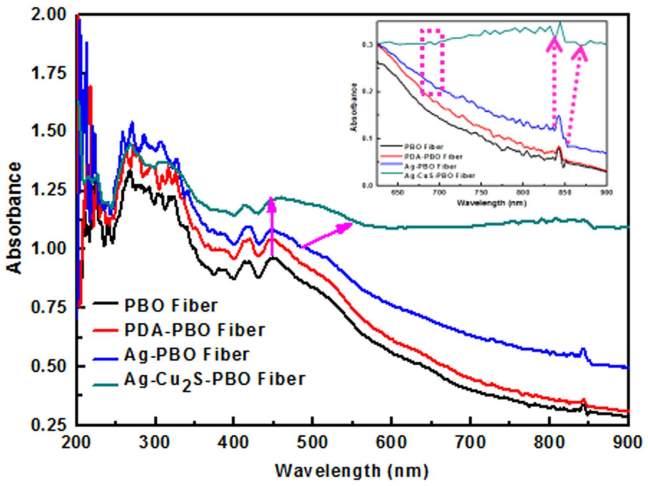

Figure 6. The UV–vis spectra of PBO, PDA–PBO, Ag–PBO, and Cu_2S–Ag–PBO fibers. The inset is the magnificated UV–vis spectra in the wavelength of 600–900 nm.

nanoparticles can be well observed. The d spacing of 0.37 and 0.13 nm can be assigned to the (202) and (106) lattice plane of the monoclinic Cu_2S. Meanwhile, the d spacing of 0.28 and 0.26 nm can be assigned to the (004) and (101) lattice plane of the cubic Ag.

The grown Ag–Cu_2S nanoparticles onto the fiber surface gave Ag–Cu_2S–PBO fibers distinct optical properties. The light absorption ability of PBO fibers was determined by UV–vis spectroscopy and shown in figure 6. The pristine PBO fibers showed characteristic absorption peaks located at ~260 and ~410 nm. Previous reports have indicated that the PDA and Ag nanoparticles were beneficial to light-thermal energy conversion and storage [35]. Fortunately, both the PDA–PBO and Ag–PBO fibers exhibited much stronger absorbance than the pristine PBO fibers in the visible region, which was very important for the photothermal conversion efficiency. It was the fact that the surface plasmon resonance absorption band of Ag nanoparticles was dependent on the size and mainly located in the range of 400–450 nm [56, 57]. However, the absorption peak for Ag was not detected in the UV–vis spectrum, probably because it was too weak and overlapped with the absorbance of PBO fibers. After deposition of Cu_2S nanoparticles on the surface of Ag–PBO fibers, another absorption peak at 688 nm was observed and was ascribed to the Cu_2S nanoparticles absorption [58]. Specifically, the absorption range of the Ag–Cu_2S–PBO fibers was extended to the near infrared region, which was a result of the plasmon-to-exciton/plasmon coupling effect between the Ag and Cu_2S nanoparticles. Consequently, the Ag–Cu_2S–PBO fibers possessed excellent light absorption performance and transformed light energy into heat effectively.

As an efficient photoabsorber in the visible region, Ag–Cu_2S nanoparticles were expected to be good nanoheaters for interfacial damage self-healing of PBO fiber composites. To verify the photothermal effect of Ag–Cu_2S nanoparticles, the temperature change of 100 ml of Ag–Cu_2S solution (1.25 g l^{-1}) was monitored under the irradiation of Xe light (the schematic illustration is shown in figure S7). The

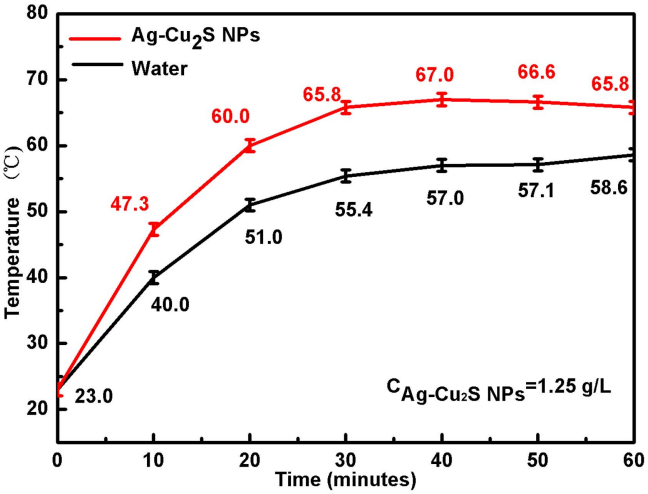

Figure 7. Temperature elevation of Ag–Cu_2S nanoparticles solution as a function of Xe light irradiation time.

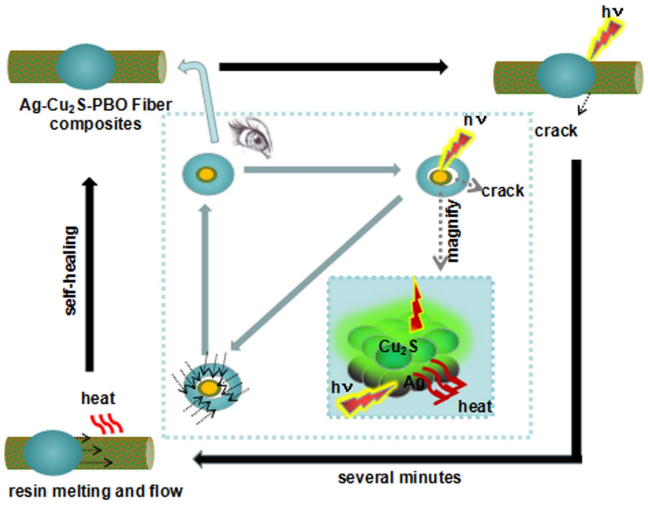

Figure 8. Light-triggered self-healing interface of Ag–Cu_2S–PBO fiber composite.

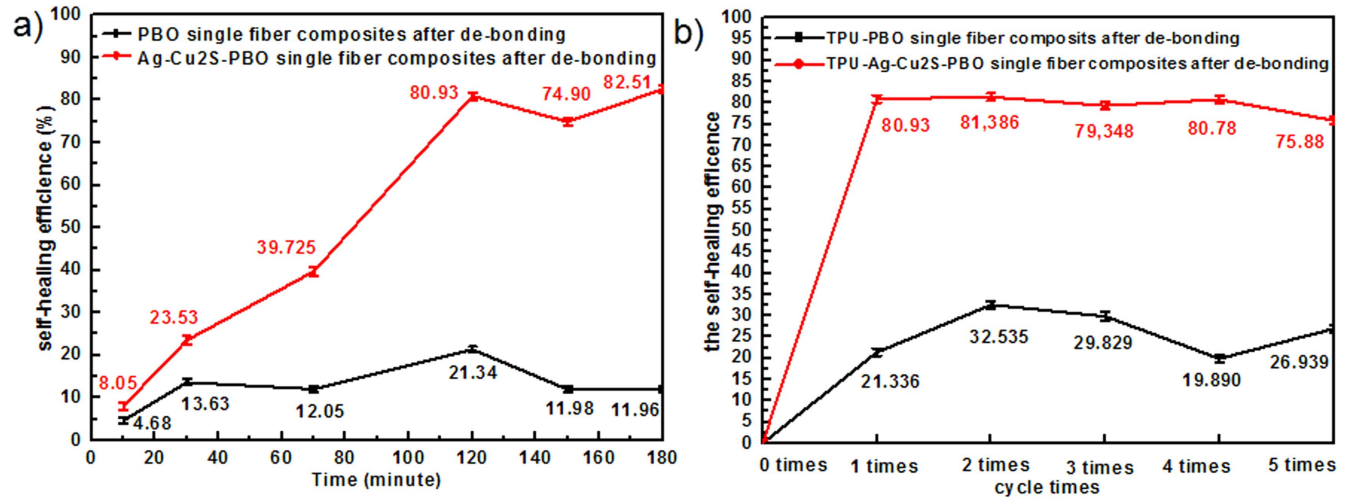

Figure 9. (a) The self-healing efficiency of Ag–Cu_2S–PBO fiber composites after Xe light irradiation for different time periods; (b) variation of the self-healing efficiency of the Ag–Cu_2S–PBO fiber composites over five cycles.

temperature elevation of the Ag–Cu_2S solution was measured as a function of time (figure 7). With the Xe light irradiation for 30 min, the solution temperature increased from 23.0 °C to 65.8 °C, which was ascribed to the effective photon capture ability of Ag–Cu_2S nanoparticles. As a contrast, the temperature of pure water showed less increase from 23.0 °C to 55.4 °C. The temperature increasing rate of Ag–Cu_2S was higher than pure water, which indicated Ag–Cu_2S possessed excellent photothermal conversion properties.

It has been experimentally confirmed that the Ag–Cu_2S nanoparticles will be an ideal light-triggered self-healing agent for PBO fibers. In order to understand the possible mechanism of interfacial self-healing of PBO fiber composites, the model of de-bonding TPU–Ag–Cu_2S–PBO single fiber composite was used. The possible mechanism of interfacial self-healing of PBO fiber composites is illustrated in figure 8. The de-bonding TPU–Ag–Cu_2S–PBO single fiber composite was exposed to Xe light irradiation. The Ag–Cu_2S absorbed the light energy and converted it to heat. As the local temperature was increased to the T_g of TPU, the TPU droplet started to diffuse across the damaged interface and healed the damage. Moreover, the thermal imager was used to assess the surface temperature of the Ag–Cu_2S–PBO fiber as it varies with time in the process of photothermal self-healing. As shown in figure S8, the PBO fiber surface temperature changed from 13.4 °C to 118.6 °C under the Xe light irradiation for 120 min. The result illustrated that the Ag–Cu_2S nanoparticles play a key role in the process of the interfacial self-healing.

To quantify the interfacial self-healing properties, IFSS tests were performed on the original and self-healed composites. As shown in figure 9(a), there was no significant change in the self-healing efficiency of the debonding single TPU–PBO fiber composite under the light irradiation. However, the interfacial self-healing efficiency of the TPU–Ag–Cu_2S–PBO fiber composite was gradually increased to 80.97% with the light irradiation time up to 120 min. Due to the mechanism of the present light-triggered self-healing strategy, the interface damage can theoretically be repaired indefinitely. In this work, the interfacial damage of TPU–Ag–Cu_2S–PBO fiber composites could be repeatedly self-healed for more than five times and the efficiency in each healing cycle was maintained at 75%–81% (figure 9(b)).

To get the detailed and convincing evidences for the interfacial self-healing behaviors, SEM images were taken. As shown in figures 10(a) and (b), both the PBO fibers and Ag–Cu_2S–PBO fibers were completely intact with the TPU droplet before debonding. After droplet debonding, apparent microcrack between the TPU resin and PBO fibers was observed in the interface of the deformed TPU–PBO fibers (figure 10(c)) and Ag–Cu_2S–PBO fibers (figure 10(d)). Furthermore, the PBO fibers and Ag–Cu_2S–PBO fibers were exposed at the debonding position. The debonding position of the pristine PBO fibers was almost clean (figure 10(c)). However, there were lots of TPU fragments and microcracks in the debonding position of the Ag–Cu_2S–PBO fibers (figure 10(d)). These results might indicate that the adhesive force between TPU and Ag–Cu_2S–PBO fibers was stronger. After light-triggered self-healing with Xe light, there was no obvious change on the morphology of the deformed TPU–PBO fibers (figure 10(e)). Compared with the PBO fibers, the deformed TPU–Ag–Cu_2S–PBO fibers were significantly healed at the debonding position (figure 10(f)). A new interface between the Ag–Cu_2S–PBO fibers and the TPU resin was formed by the mechanical interlock. Additionally, it can be clearly seen that the structure of the TPU droplet and PBO fiber has no obvious change after 120 min Xe light irradiation (figures 10(e) and (f)). It can be sure that the resin is partially melted at ~120 °C. Owing to good photothermal properties of the Ag–Cu_2S, the resin of the contact part of the interface quickly reached the glass transition temperature. Then the interface crack was healed. These results demonstrate that Ag–Cu_2S–PBO fiber composites can be self-healed by Xe light irradiation.

To characterize mechanical properties, TS and IFSS were evaluated in the present study [59]. As shown in figure 11, the TS and IFSS of the pristine PBO fibers were 5.82 GPa and 65.67 MPa, respectively. After PDA modification, the TS of PDA–PBO fiber had a small decrease to 5.61 GPa because of the acid corrosion during the sizing process, and the IFSS

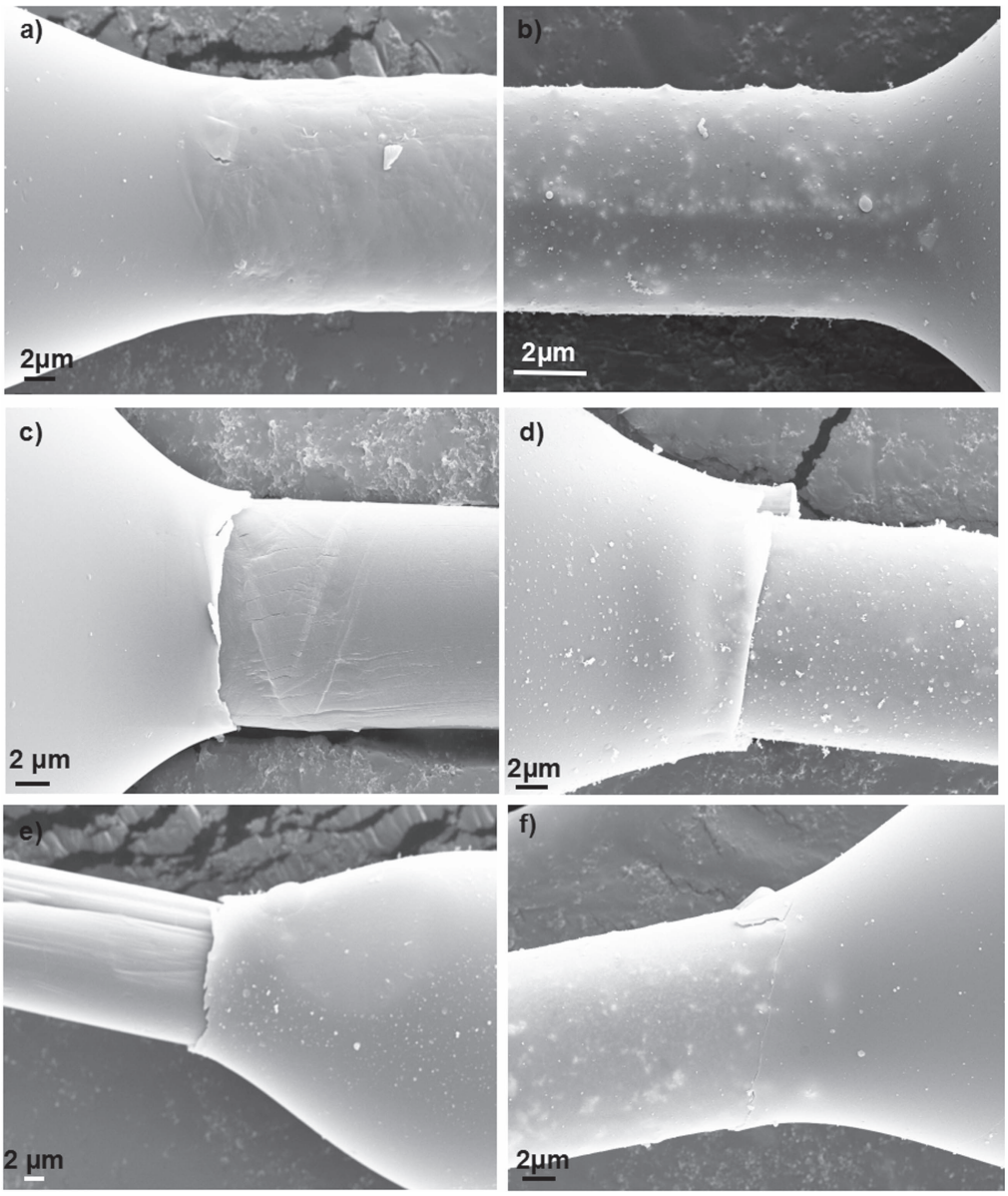

Figure 10. SEM images of (a) PBO fiber composite, (b) Ag–Cu_2S–PBO fiber composite, (c) PBO fiber after the TPU droplet debonding, (d) Ag–Cu_2S–PBO fiber after the TPU droplet debonding, (e) PBO fiber composite after Xe light irradiation, (f) Ag–Cu_2S–PBO fiber composite after Xe light irradiation.

increased to 67.68 MPa. Compared with PDA–PBO fiber, the TS of Ag–PBO fiber was 5.56 GPa. The result indicated that the microwave irradiation had no negative influence on the TS of Ag–PBO fibers. Meanwhile, the IFSS had a slight increase to 76.06 MPa due to abundant Ag on the surface of PDA–PBO fibers that provided more chances to contact with the resins. It can be seen that the TS of the Ag–Cu_2S–PBO fibers was not negatively influenced by the Cu_2S growth process. In addition, it is worth noting that the IFSS of the Ag–Cu_2S–PBO fiber was 72.34 MPa, which was higher than the pristine PBO fibers and lower than Ag–PBO fibers. For Ag–PBO fibers, the mechanical interlocking increased with increasing the content of loaded-nanoparticles. However, with the continuous increase in the content of nanoparticles, some nanoparticles may aggregate on PBO fibers, leading to a slight decrease in IFSS. It is the fact that PBO fibers, like other high strength organic fibers, are sensitive

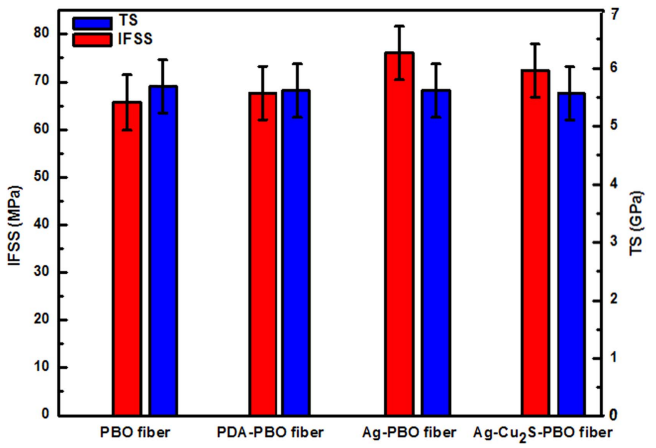

Figure 11. IFSS and TS value of modified PBO fibers.

to UV exposure, which can deteriorate the mechanical properties of PBO fibers and corresponding composites. In the future, the method of layer-by-layer modification will be taken to solve the problem, such as the anti-UV coating will be also deposited on the fibers for protection of PBO fibers from UV aging.

4. Conclusion

In the present study, novel Ag–Cu_2S–PBO fibers with light-triggered self-healing properties were designed and prepared. The dopamine chemistry and further immobilization process firmly anchored the Ag–Cu_2S nanoparticles on the PBO fibers without causing any significantly negative effect on the mechanical properties. Under Xe light irradiation, the Ag–Cu_2S efficiently raised the temperature at the interface, which recovered the 80.93% IFSS of the debonded composites. Moreover, the self-healing efficiencies were kept at ∼80% throughout five repeated cycles. The present study provides a novel strategy to achieve the self-healing of interfacial damage, which can be widely used in the composite science.

Acknowledgments

We thank the National Natural Science Foundation of China (no. 51673053), the Natural Science Foundation of Heilongjiang Province (no. LC2017024), and the Fundamental Research Funds for the Central Universities (no. HIT. IBR-SEM. 2013016).

ORCID iDs

Zhen Hu https://orcid.org/0000-0002-0160-782X

References

[1] Awaja F, Zhang S N, Tripathi M, Nikiforov A and Pugno N 2016 Cracks, microcracks and fracture in polymer structures: formation, detection, autonomic repair *Prog. Mater. Sci.* **83** 536–73
[2] Zhong N and Wouter Post W 2015 Self-repair of structural and functional composites with intrinsically self-healing polymer matrices: a review *Composites* A **69** 226–39
[3] Skorb E V and Möhwald H 2013 25th anniversary article: dynamic interfaces for responsive encapsulation systems *Adv. Mater.* **25** 5029–43
[4] Mei H, Zhang S M, Chen H, Zhou H S, Zhai X Y and Cheng L F 2016 Interfacial modification and enhancement of toughening mechanisms in epoxy composites with CNTs grafted on carbon fibers *Compos. Sci. Technol.* **134** 89–95
[5] Zhang W, Duchet J and Gérard J F 2016 Effect of epoxy matrix architecture on the self-healing ability of thermo-reversible interfaces based on Diels–Alder reactions: demonstration on a carbon fiber/epoxy microcomposite *RSC Adv.* **6** 114235–43
[6] Zhang W, Duchet J and Gérard J F 2014 Self-healable interfaces based on thermo-reversible Diels–Alder reactions in carbon fiber reinforced composites *J. Colloid Interface Sci.* **430** 61–8
[7] Jin F L and Park S J 2015 Preparation and characterization of carbon fiber-reinforced thermosetting composites: a review *Carbon Lett.* **2** 67–77
[8] Wu X F and Yarin A L 2013 Recent progress in interfacial toughening and damage self-healing of polymer composites based on electrospun and solution-blown nanofibers: an overview *J. Appl. Polym. Sci.* **130** 2225–37
[9] Yang Y, Ding X C and Urban M W 2015 Chemical and physical aspects of self-healing materials *Prog. Polym. Sci.* **49–50** 34–59
[10] Wu D Y, Meure S and Solomon D 2008 Self-healing polymeric materials: a review of recent developments *Prog. Polym. Sci.* **33** 479–522
[11] Xu G X, Huang Z H, Chen P Y, Cui T Q, Zhang X H, Miao B and Yan L T 2017 Optimal reactivity and improved self-healing capability of structurally dynamic polymers grafted on janus nanoparticles governed by chain stiffness and spatial organization *Small* **13** 1603155
[12] Bekas D G, Tsirka K, Baltzis D and Paipetis A S 2016 Self-healing materials: a review of advances in materials, evaluation, characterization and monitoring techniques *Composites* B **87** 92–119
[13] Ji S B, Cao W, Yu Y and Xu H P 2015 Visible-light-induced self-healing diselenide-containing polyurethane elastomer *Adv. Mater.* **27** 7740–5
[14] Wool R P 2008 Self-healing materials: a review *Soft Matter* **4** 400–18
[15] Zhu D Y, Rong M Z and Zhang M Q 2015 Self-healing polymeric materials based on microencapsulated healing agents: from design to preparation *Prog. Polym. Sci.* **49–50** 175–220
[16] Shchukin D G 2013 Container-based multifunctional self-healing polymer coatings *Polym. Chem.* **4** 4871–7
[17] Toohey K S, Sottos N R, Lewis J A, Moore J S and White S R 2007 Self-healing materials with microvascular networks *Nat. Mater.* **6** 581–6
[18] Gordon M B, French J M, Wagner N J and Kloxin C J 2015 Dynamic bonds in covalently crosslinked polymer networks for photoactivated strengthening and healing *Adv. Mater.* **27** 8007–10
[19] Zhang H J and Zhao Y 2013 Polymers with dual light-triggered functions of shape memory and healing using gold nanoparticles *ACS Appl. Mater. Interfaces* **5** 13069–75
[20] Habault D, Zhang H J and Zhao Y 2013 Light-triggered self-healing and shape-memory polymers *Chem. Soc. Rev.* **42** 7244–56
[21] Huang L, Yi N B, Wu Y P, Zhang Y, Zhang Q, Huang Y, Ma Y F and Chen Y S 2013 Multichannel and repeatable self-healing of mechanical enhanced graphene-thermoplastic polyurethane composites *Adv. Mater.* **25** 2224–8
[22] Qin W Z, Vautard F, Askeland P, Yu J R and Drzal L 2015 Modifying the carbon fiber-epoxy matrix interphase with silicon dioxide nanoparticles *RSC Adv.* **5** 2457–65
[23] Fu G L, Sanjay S T, Dou M W and Li X J 2016 Nanoparticle-mediated photothermal effect enables a new method for quantitative biochemical analysis using a thermometer *Nanoscale* **8** 5422–7
[24] Hu J, Wang H Q, Dong F and Wu Z B 2017 A new strategy for utilization of NIR from solar energy-promotion effect generated from photothermal effect of Fe_3O_4 @ SiO_2 for photocatalytic oxidation of NO *Appl. Catal.* B **204** 584–92
[25] Xiao J W, Fan S X, Wang F, Sun L D, Zheng X Y and Yan C H 2014 Porous Pd nanoparticles with high photothermal conversion efficiency for efficient ablation of cancer cells *Nanoscale* **6** 4345–51
[26] Hu Z, Wang C, Zhao F, Xu X, Wang S, Yu L, Zhang D and Huang Y 2017 Fabrication of a graphene/C_{60} nanohybrid via gamma-cyclodextrin host-guest chemistry for photodynamic and photothermal therapy *Nanoscale* **9** 8825–33

[27] Hu Z, Zhang D, Yu L and Huang Y 2018 Light-triggered C_{60} release from a graphene/cyclodextrin nanoplatform for the protection of cytotoxicity induced by nitric oxide *J. Mater. Chem.* B **6** 518–26

[28] Chen X, Dam M A, Ono K, Mal A, Shen H, Nutt S R, Sheran K and Wudl F 2002 A thermally remendable cross-linked polymeric material *Science* **295** 1698–702

[29] Burnworth M, Tang L, Kumpfer J R, Duncan A J, Beyer F L, Fiore G L, Rowan S J and Weder C 2011 Stress transfer in cellulose nanowhisker composites influence of whisker aspect ratio and surface charge *Nature* **472** 334–7

[30] Chen L, Hu Z, Wu Z J, Wu G S, Ma L C, Zhang C H and Huang Y D 2017 POSS-bound ZnO nanowires as interphase for enhancing interfacial strength and hydrothermal aging resistance of PBO fiber/epoxy resin composites *Composites* A **96** 1–8

[31] Hu Z, Shao Q, Moloney M G, Xu X, Zhang D, Li J, Zhang C and Huang Y 2017 Nondestructive functionalization of graphene by surface-initiated atom transfer radical polymerization: an ideal nanofiller for poly(p-phenylene benzobisoxazole) fibers *Macromolecules* **50** 1422–9

[32] Sun J F, Zhao F, Yao Y, Jin Z, Liu X and Huang Y D 2017 High efficient and continuous surface modification of carbon fibers with improved tensile strength and interfacial adhesion *Appl. Surf. Sci.* **412** 425–35

[33] Zhang L B, Tang B, Wu J B, Li Y and Wang P 2015 Hydrophobic light-to-heat conversion membranes with self-healing ability for interfacial solar heating *Adv. Mater.* **27** 4889–94

[34] Wang C F, Li J, Sun S F, Li X Y, Wu G S, Wang Y W, Xie F and Huang Y D 2016 Controlled growth of silver nanoparticles on carbon fibers for reinforcement of both tensile and interfacial strength *RSC Adv.* **6** 14016–26

[35] Liu X J, Li B, Fu F F, Xu K B, Zou R J, Wang Q, Zhang B J, Chen Z G and Hu J Q 2014 Facile synthesis of biocompatible cysteine-coated CuS nanoparticles with high photothermal conversion efficiency for cancer therapy *Dalton Trans.* **43** 11709–15

[36] Liu X J, Ren Q L, Fu F F, Zou R J, Wang Q, Xin G B, Xiao Z Y, Huang X J, Liu Q and Hu J Q 2015 CuS @ $mSiO_2$-PEG core–shell nanoparticles as a NIR light responsive drug delivery nanoplatform for efficient chemo-photothermal therapy *Dalton Trans.* **44** 10343–51

[37] Liu X L, Fu F F, Xu K B, Zou R J, Yang J M, Wang Q, Liu Q, Xiao Z Y and Hu J Q 2014 Folic acid-conjugated hollow mesoporous silica/CuS nanocomposites as a difunctional nanoplatform for targeted chemo-photothermal therapy of cancer cells *J. Mater. Chem.* B **2** 5358–67

[38] Li B, Wang Q, Zou R J, Liu X J, Xu K B, Li W Y and Hu J Q 2014 $Cu_{7.2}S_4$ nanocrystals: a novel photothermal agent with a 56.7% photothermal conversion efficiency for photothermal therapy of cancer cells *Nanoscale* **6** 3274–82

[39] Zhong R Z, Peng C, Chen L, Yu N, Liu Z X, Zhu M F, He C L and Chen Z G 2016 Egg white-mediated green synthesis of CuS quantum dots as a biocompatible and efficient 980 nm laser-driven photothermal agent *RSC Adv.* **6** 40480–8

[40] Peng L H, Guo R H, Lan J W, Jiang S X and Lin S J 2016 Microwave-assisted deposition of silver nanoparticles on bamboo pulp fabric through dopamine functionalization *Appl. Surf. Sci.* **386** 151–9

[41] Qiu B, Xu C X, Sun D Z, Wei H G, Zhang X, Guo J, Wang Q, Rutman D, Guo Z H and Wei S Y 2014 Polyaniline coating on carbon fiber fabrics for improved hexavalent chromium removal *RSC Adv.* **4** 29855–65

[42] Guo X, Cao G L, Ding F, Li X Y, Zhen S Y, Xue Y F, Yan Y M, Liu T and Sun K N 2015 A bulky and flexible electrocatalyst for efficient hydrogen evolution based on the growth of MoS_2 nanoparticles on carbon nanofiber foam *J. Mater. Chem.* A **3** 5041–6

[43] Jha A, Sarkar S K, Sen D and Chattopadhyay K K 2015 A carbon fiber-ZnS nanocomposite for dual application as an efficient cold cathode as well as a luminescent anode for display technology *Nanoscale* **7** 2536–44

[44] Ma J F, Fu W F, Meng Y Q, Yu Z Q, Cai S and Niu B B 2016 'Electrochemical' growth of ZnO coating on carbon fiber *Mater. Chem. Phys.* **171** 22–6

[45] Shi G, Ju S, Huang C F, Jiang D Z and Zhang J W 2015 Tensile strength of surface treated PBO fiber *Mater. Sci. Forum* **815** 622–8

[46] Wu G S, Ma L C, Wang Y W, Liu L and Huang Y D 2016 Improvements in interfacial and heat-resistant properties of carbon fiber/methylphenylsilicone resins composites by incorporating silica-coated multi-walled carbon nanotubes *J. Adhes. Sci. Technol.* **2** 117–30

[47] Yang J, Qi G Q, Tang L S, Bao R Y, Bai L, Liu Z Y, Yang W, Xie B H and Yang M B 2016 Novel photo driven composite phase change materials with bioinspired modification of BN for solar-thermal energy conversion and storage *J. Mater. Chem.* A **4** 9625–34

[48] Zheng N, Huang Y D, Sun W F, Du X S, Liu H Y, Moody S, Gao J F and Mai Y W 2016 *In situ* pull-off of ZnO nanowire from carbon fiber and improvement of interlaminar toughness of hierarchical ZnO nanowire/carbon fiber hybrid composite laminates *Carbon* **110** 69–78

[49] Wu X J, Zhou L Z, Su Y and Dong C M 2016 A polypeptide micelle template method to prepare polydopamine composite nanoparticles for synergistic photothermal-chemotherapy *Polym. Chem.* **7** 5552–62

[50] Wang W C, Li R Y, Tian M, Liu L, Zou H, Zhao X Y and Zhan L Q 2013 Surface silverized meta-aramid fibers prepared by bio-inspired poly (dopamine) functionalization *ACS Appl. Mater. Interfaces* **5** 2062–9

[51] Ding X G *et al* 2014 Surface plasmon resonance enhanced light absorption and photothermal therapy in the second near-infrared window *J. Am. Chem. Soc.* **136** 15684–93

[52] Tian J L, Zhang W, Gu J J, Deng T and Zhang D 2015 Bioinspired Au-CuS coupled photothermal materials: enhanced infrared absorption and photothermal conversion from butterfly wings *Nano Energy* **17** 52–62

[53] Hu G F, Xu T T, Chen X Q, James T D and Xu S Y 2016 Solar-driven broad spectrum fungicides based on monodispersed Cu_7S_4 nanorods with strong near-infrared photothermal efficiency *RSC Adv.* **6** 103930–7

[54] Zhang Q B, Wu G S, Xie F, Li N, Huang Y D and Liu L 2014 Mechanical properties of carbon fiber composites modified with nano-SiO_2 in the interphase *J. Adhes. Sci. Technol.* **28** 2154–66

[55] Wang M Q, Wang C Y, Song Y J, Xie H Q and Huang Y D 2017 One-pot *in situ* polymerization of graphene oxide nanosheets and poly (p-phenylenebenzobisoxazole) with enhanced mechanical and thermal properties *Compos. Sci. Technol.* **14** 16–23

[56] Yang K H, Hsu S C and Huang M H 2016 Facet-dependent optical and photothermal properties of Au @ Ag-Cu_2O core–shell nanocrystals *Chem. Mater.* **28** 5140–6

[57] Chen M J, He Y R, Huang J and Zhu J Q 2016 Synthesis and solar photo-thermal conversion of Au, Ag, and Au–Ag blended plasmonic nanoparticles *Energy Convers. Manage.* **127** 293–300

[58] Shi Y H, Chen Y J, Tian G H, Wang L Y, Xiao Y T and Fu H G 2015 Hierarchical Ag/Ag_2S/CuS ternary heterostructure composite as an efficient visible-light photocatalyst *ChemCatChem* **7** 1684–90

[59] Hu Z, Shao Q, Xu X, Zhang D and Huang Y 2017 Surface initiated grafting of polymer chains on carbon nanotubes via one-step cycloaddition of diarylcarbene *Compos. Sci. Technol.* **142** 294–301